Unconditionally stable algorithms to solve the time-dependent Maxwell equations

J. S. Kole,* M. T. Figge,† and H. De Raedt‡
Centre for Theoretical Physics and Materials Science Centre, University of Groningen, Nijenborgh 4, NL-9747 AG Groningen, The Netherlands
(Received 3 July 2001; published 27 November 2001)

Based on the Suzuki product-formula approach, we construct a family of unconditionally stable algorithms to solve the time-dependent Maxwell equations. We describe a practical implementation of these algorithms for one-, two-, and three-dimensional systems with spatially varying permittivity and permeability. The salient features of the algorithms are illustrated by computing selected eigenmodes and the full density of states of one-, two-, and three-dimensional models and by simulating the propagation of light in slabs of photonic band-gap materials.

DOI: 10.1103/PhysRevE.64.066705 PACS number(s): 02.60.Cb, 03.50.De, 41.20.Jb, 42.70.Qs

I. INTRODUCTION

Maxwell's partial differential equations of electromagnetism describe the evolution of electric and magnetic fields in time and space [1]. They apply to a wide range of different physical situations that are specified by the boundary conditions on the electromagnetic (EM) fields. In many cases, numerical methods are required to solve Maxwell's equations, either in the frequency or time domain. For the time domain, a well-known class of algorithms is based on a method proposed by Yee [2] and is called the finite-difference time-domain (FDTD) method. The FDTD method has matured during past years and various algorithms implemented for specific purposes are available by now [3,4]. These algorithms owe their popularity mainly due to their flexibility and speed, while at the same time, they are easy to implement. A limitation of Yee-based FDTD techniques is that the stability of the algorithms is conditional. The stability depends on the mesh size used to discretize space and the time step used to perform the time integration [3].

In this paper, we present a family of unconditionally stable algorithms that solve the time-dependent Maxwell equations (TDME) through the application of orthogonal transformations. That this is possible follows from the representation of the TDME in matrix form. The exponential of a skew-symmetric matrix plays the role of the time-evolution operator of the EM fields. This time-evolution operator is orthogonal. The key to the construction of an unconditionally stable algorithm to solve the Maxwell equations is the observation that orthogonal approximations to this operator automatically yield unconditionally stable algorithms. The Lie-Trotter-Suzuki product formulas [5] provide the mathematical framework to construct orthogonal approximations to the time-evolution operator of the Maxwell equations. However, this framework does not specify how to implement the algorithm.

Recently, a spectral-domain split-operator technique has been proposed to solve the TDME [6]. The split-operator approach is based on one of the many forms of the Lie-Trotter-Suzuki product formulas. The spectral-domain method makes use of fast Fourier transforms to compute the matrix exponentials of the displacement operators. The choice made in Ref. [6] yields an approximation to the time-evolution operator that is no longer orthogonal and hence unconditional stability is not automatically guarantueed [7]. In contrast, the methodology that we propose yields efficient, explicit, unconditionally stable schemes that operate on the EM fields defined on the real-space grid only. This renders the algorithms rather flexible, avoids wrap-around effects [6], and naturally allows for the spatial variations in both the permittivity and the permeability. On the other hand, the implementation described in this paper is by no means unique and leaves a lot of room for further improvements.

For EM fields in a homogeneous medium, Zheng *et al.* and Zheng and Chen showed that there is an alternating-direction-implicit time stepping algorithm that is unconditionally stable [8,9]. Conceptually, this approach is different from ours. The Fourier-mode stability analysis performed by Zheng *et al.* [8] does not generalize to the case of spatially varying permittivity and permeability, whereas in our approach, the algorithms are unconditionally stable by construction.

Our presentation is organized as follows: The basic theoretical concepts are given in Sec. II. In Sec. III, we explain the general philosophy that underlies the Suzuki approach to construct algorithms that are unconditionally stable. In Sec. IV, we show in detail how to implement these ideas for the case of the TDME in one, two, and three spatial dimensions, using algorithms that are accurate up to second and fourth order in the time step. In Sec. V, we explain how we analyze the data generated by these algorithms. In Sec. VI, we present the results of numerical simulations for the physical systems that we selected as examples to test the algorithms. Our conclusions are given in Sec. VII.

II. THEORY

The model system we consider in this paper describes EM fields in a d-dimensional ($d=1,2,3$) medium with spatially varying permittivity and/or permeability, surrounded by a

*Email address: j.s.kole@phys.rug.nl
†Email address: m.t.figge@phys.rug.nl
‡Email address: deraedt@phys.rug.nl
http://rugth30.phys.rug.nl/compphys

perfectly conducting box. In the absence of free charges and currents, the EM fields in such a system satisfy Maxwell's equations [1]

$$\frac{\partial}{\partial t}\mathbf{H} = -\frac{1}{\mu}\nabla\times\mathbf{E}, \tag{1}$$

$$\frac{\partial}{\partial t}\mathbf{E} = \frac{1}{\varepsilon}\nabla\times\mathbf{H}, \tag{2}$$

$$\mathrm{div}\,\varepsilon\mathbf{E} = 0, \tag{3}$$

$$\mathrm{div}\,\mathbf{H} = 0, \tag{4}$$

where $\mathbf{H}=[H_x(\mathbf{r},t),H_y(\mathbf{r},t),H_z(\mathbf{r},t)]^T$ and $\mathbf{E}=[E_x(\mathbf{r},t),E_y(\mathbf{r},t),E_z(\mathbf{r},t)]^T$ denote the magnetic- and electric-field vector, respectively. The permeability and the permittivity are given by $\mu=\mu(\mathbf{r})$ and $\varepsilon=\varepsilon(\mathbf{r})$. For simplicity of notation, we will omit the spatial dependence on $\mathbf{r}=(x,y,z)^T$ unless this leads to ambiguities. On the surface of the perfectly conducting box, the EM fields satisfy the boundary conditions [1]

$$\mathbf{n}\times\mathbf{E}=\mathbf{0}, \quad \mathbf{n}\cdot\mathbf{H}=0, \tag{5}$$

with $\mathbf{n}$ denoting the vector normal to a boundary of the surface. The conditions Eq. (5) assure that the normal component of the magnetic field and the tangential components of the electric field vanish at the boundary [1]. Some important symmetries of the Maxwell Eqs. (1)–(4) can be made explicit by introducing the fields

$$\mathbf{X}(t)=\sqrt{\mu}\mathbf{H}(t), \quad \mathbf{Y}(t)=\sqrt{\varepsilon}\mathbf{E}(t). \tag{6}$$

In terms of the fields $\mathbf{X}(t)$ and $\mathbf{Y}(t)$, the TDME [Eqs. (1) and (2)] read

$$\frac{\partial}{\partial t}\begin{pmatrix}\mathbf{X}(t)\\ \mathbf{Y}(t)\end{pmatrix} = \begin{pmatrix} 0 & -\frac{1}{\sqrt{\mu}}\nabla\times\frac{1}{\sqrt{\varepsilon}} \\ \frac{1}{\sqrt{\varepsilon}}\nabla\times\frac{1}{\sqrt{\mu}} & 0 \end{pmatrix}\begin{pmatrix}\mathbf{X}(t)\\ \mathbf{Y}(t)\end{pmatrix} \equiv \mathcal{H}\begin{pmatrix}\mathbf{X}(t)\\ \mathbf{Y}(t)\end{pmatrix}. \tag{7}$$

Writing $\Psi(t)=[\mathbf{X}(t),\mathbf{Y}(t)]^T$, Eq. (7) becomes

$$\frac{\partial}{\partial t}\Psi(t)=\mathcal{H}\Psi(t). \tag{8}$$

It is easy to show that $\mathcal{H}$ is skew symmetric, i.e., $\mathcal{H}^T=-\mathcal{H}$, with respect to the *inner product*

$$\langle\Psi|\Psi'\rangle \equiv \int_V \Psi^T\cdot\Psi' d\mathbf{r}, \tag{9}$$

where V denotes the volume of the enclosing box.

The formal solution of Eq. (8) is given by

$$\Psi(t)=e^{t\mathcal{H}}\Psi(0), \tag{10}$$

where $\Psi(0)$ represents the initial state of the EM fields and the operator

$$U(t)=e^{t\mathcal{H}}, \tag{11}$$

determines their time evolution. By construction

$$\|\Psi(t)\|^2=\langle\Psi(t)|\Psi(t)\rangle=\int_V[\varepsilon\mathbf{E}^2(t)+\mu\mathbf{H}^2(t)]d\mathbf{r}, \tag{12}$$

relating the length of $\Psi(t)$ to the energy density

$$w(t)\equiv\varepsilon\mathbf{E}^2(t)+\mu\mathbf{H}^2(t), \tag{13}$$

of the EM fields [1]. From $U(t)^T=U(-t)=U^{-1}(t)=e^{-t\mathcal{H}}$, it follows that $\langle U(t)\Psi(0)|U(t)\Psi(0)\rangle=\langle\Psi(t)|\Psi(t)\rangle=\langle\Psi(0)|\Psi(0)\rangle$. Hence, the time-evolution operator $U(t)$ is an orthogonal transformation, rotating the vector $\Psi(t)$ without changing its length $\|\Psi\|$. In physical terms, this means that the energy density of the EM fields does not change with time, as expected on physical grounds [1].

The fact that $U(t)$ is an orthogonal transformation is essential for the development of an unconditionally stable algorithm to solve the Maxwell equations. In practice, a numerical procedure solves the TDME by making use of an approximation $\tilde{U}(t)$ to the true time evolution $U(t)$ (see below). A necessary and sufficient condition for an algorithm to be unconditionally stable is that [10]

$$\|\tilde{U}(t)\Psi(0)\|\leqslant\|\Psi(0)\|. \tag{14}$$

In other words, the length of $\Psi(t)$ should be bounded, for arbitrary initial condition $\Psi(t=0)$ and for any time t [10]. By choosing for $\Psi(0)$ the eigenvector of $\tilde{U}(t)$ that corresponds to the largest eigenvalue of $\tilde{U}(t)$, it follows from Eq. (14) that the algorithm will be unconditionally stable by construction if and only if the largest eigenvalue of $\tilde{U}(t)$ (denoted by $\|\tilde{U}(t)\|$) is less or equal than one [10]. If the approximation $\tilde{U}(t)$ is itself an orthogonal transformation, then $\|\tilde{U}(t)\|=1$ and the numerical scheme will be unconditionally stable.

In summary, unconditionally stable algorithms to solve Eq. (7) may be constructed by employing orthogonal approximations to the time-evolution $U(t)=e^{t\mathcal{H}}$. For the case at hand, unconditional stability is tantamount to the exact conservation of the energy density.

III. UNCONDITIONALLY STABLE ALGORITHMS

A numerical procedure that solves the TDME necessarily starts by discretizing the spatial derivatives (see Sec. IV). This maps the continuum problem described by $\mathcal{H}$ onto a lattice problem defined by a matrix H. Ideally, this mapping should not change the basic symmetries of the original problem. The underlying, symmetry of the TDME suggests the use of matrices H that are real and skew symmetric. For-

mally, the time evolution of the EM fields on the lattice is given by

$$\Psi(t+\tau)=U(\tau)\Psi(t)=e^{\tau H}\Psi(t). \tag{15}$$

The second ingredient of the numerical procedure is to choose an approximation of the time-step operator $U(\tau)$. A standard procedure is to truncate the Taylor series of the matrix exponential [11,12]

$$U(\tau)=e^{\tau H}=\sum_{n=0}^{\infty}\frac{(\tau H)^n}{n!}. \tag{16}$$

Retaining terms up to first order in τ yields

$$\tilde{U}(\tau)=I+\tau H, \tag{17}$$

where I denotes the identity operator. As $\tilde{U}(\tau)\tilde{U}(\tau)^T=I-(\tau H)^2\neq I$ for $\tau\neq 0$, it is clear that the matrix Eq. (17) is not orthogonal. Making use of the symmetry of H and the positivity of the inner product, we find that

$$\begin{aligned}\langle\Psi(\tau)|\Psi(\tau)\rangle&=\langle\tilde{U}(\tau)\Psi(0)|\tilde{U}(\tau)\Psi(0)\rangle\\&=\langle\Psi(0)|\Psi(0)\rangle+\tau^2\langle H\Psi(0)|H\Psi(0)\rangle\\&>\langle\Psi(0)|\Psi(0)\rangle,\end{aligned}$$

implying that Eq. (14) does not hold. Hence, according to the arguments given above, the (Euler) scheme Eq. (17) is unstable, a fact that is, of course, well known [10].

The Yee algorithm is based on a leapfrog arrangement [2] and formally corresponds to an approximation to the matrix exponential $U(\tau)$ that may be written as

$$\tilde{U}_{\mathrm{Yee}}(\tau)=I+\tau H_1+\tau^2 H_2, \tag{18}$$

where H_1 and H_2 are matrices, the structure of which depends on the lattice dimensionality. The presence of the second-order contribution may render the algorithm stable under certain conditions. It seems difficult to determine these conditions for arbitrary (skew-symmetric) H_1 and (symmetric) H_2, i.e., without making use of very specific knowledge about the elements of H_1 and H_2. For EM fields moving in free space, a Fourier-space stability analysis of the Yee algorithm yields

$$\tau\leqslant\frac{\Delta}{c\sqrt{d}}, \tag{19}$$

as the condition for stability [3]. Here, c is the light velocity in vacuum, Δ denotes the spatial mesh size, and d is the dimensionality of the system.

A systematic approach to construct orthogonal approximations to matrix exponentials, i.e., to construct unconditionally stable algorithms, is to make use of the Lie-Trotter-Suzuki formula [13,14]

$$e^{t(H_1+\cdots+H_p)}=\lim_{m\to\infty}\left(\prod_{i=1}^{p}e^{tH_i/m}\right)^m, \tag{20}$$

and generalizations thereof [5,16]. Applied to the case of interest here, the success of this approach relies on the basic but rather trivial premise that the matrix H may be written as

$$H=\sum_{i=1}^{p}H_i, \tag{21}$$

where each of the matrices H_i is real and skew symmetric.

The expression Eq. (20) suggests that

$$U_1(\tau)=e^{\tau H_1}\cdots e^{\tau H_p}, \tag{22}$$

might be a good approximation to $U(\tau)$ if τ is sufficiently small. Most importantly, if all the H_i are real and skew symmetric, $U_1(\tau)$ is orthogonal by construction. Therefore, by construction, a numerical scheme based on Eq. (22) will be unconditionally stable. Using the fact that both $U(\tau)$ and $U_1(\tau)$ are orthogonal matrices, it may be shown that [17]

$$\|U(\tau)-U_1(\tau)\|\leqslant\frac{\tau^2}{2}\sum_{i<j}\|[H_i,H_j]\|, \tag{23}$$

where $[H_i,H_j]=H_iH_j-H_jH_i$. From Eq. (23) it follows that, in general, the Taylor series of $U(\tau)$ and $U_1(\tau)$ are identical up to first order in τ. We will call $U_1(\tau)$ a first-order approximation to $U(\tau)$.

The product-formula approach provides simple, systematic procedures to improve the accuracy of the approximation to $U(\tau)$ without changing its fundamental symmetries. For example the orthogonal matrix

$$U_2(\tau)=U_1(-\tau/2)^TU_1(\tau/2)=e^{\tau H_p/2}\cdots e^{\tau H_1/2}e^{\tau H_1/2}\cdots e^{\tau H_p/2}, \tag{24}$$

is a second-order approximation to $U(\tau)$ [5,16]. Suzuki's fractal decomposition approach [5] gives a general method to construct higher-order approximations based on $U_1(\tau)$ or $U_2(\tau)$. A particularly useful fourth-order approximation is given by [5]

$$U_4(\tau)=U_2(a\tau)U_2(a\tau)U_2[(1-4a)\tau]U_2(a\tau)U_2(a\tau), \tag{25}$$

where $a=1/(4-4^{1/3})$. The approximations Eqs. (22), (24), and (25) have proven to be very useful in many applications [14–25] and, as we show below, turn out to be equally useful for solving the TDME. In practice, an efficient implementation of the first-order scheme is all that is needed to construct the higher-order algorithms Eqs. (24) and (25).

To summarize, Suzuki's product-formula approach provides the formal machinery to define algorithms that are unconditionally stable by construction. The accuracy of these algorithms may be improved systematically, to any desired order [5]. The only assumption made so far is that the real, skew-symmetric matrix H representing the TDME may be written as a sum of p real, skew-symmetric matrices H_i. The

next step is to choose the H_i's such that the matrix exponentials $\exp(\tau H_1)\cdots\exp(\tau H_p)$ may be calculated efficiently. This will turn the formal expressions for $U_2(\tau)$ and $U_4(\tau)$ into efficient algorithms to solve the TDME.

IV. IMPLEMENTATION

In this section, we present the details of our implementation of unconditionally stable algorithms to solve the TDME based on the Suzuki product-formula approach. For pedagogical reasons, we start by considering the simplest case: A one-dimensional (1D) system. Then we show that the strategy adopted for 1D readily extends to higher spatial dimensions. The implementation we describe below is by no means unique, leaving a lot of room for further improvements. In principle, any decomposition Eq. (21) of H into real skew-symmetric parts will do. Largely guided by previous work [17,19,24,25], we have adopted a decomposition that is efficient, flexible, sufficiently accurate, and easy to program.

A. One dimension

We consider a 1D system along the x direction. Accordingly, Maxwell's equations contain no partial derivatives with respect to y or z and ε and μ do not depend on y or z. Under these conditions, the TDME reduce to two independent sets of first-order differential equations [1]. The solutions to these sets are known as the transverse electric (TE) mode and the transverse magnetic (TM) mode [1]. As the equations of the TE and TM mode only differ by a sign, we may restrict our considerations to the TM mode and obtain the result for the TE mode by reversing the time.

From Eq. (7) it follows that the magnetic field $H_y(x,t) = X_y(x,t)/\sqrt{\mu(x)}$ and the electric field $E_z(x,t) = Y_z(x,t)/\sqrt{\varepsilon(x)}$ of the TM mode are solutions of

$$\frac{\partial}{\partial t}X_y(x,t) = \frac{1}{\sqrt{\mu(x)}}\frac{\partial}{\partial x}\left(\frac{Y_z(x,t)}{\sqrt{\varepsilon(x)}}\right), \tag{26}$$

$$\frac{\partial}{\partial t}Y_z(x,t) = \frac{1}{\sqrt{\varepsilon(x)}}\frac{\partial}{\partial x}\left(\frac{X_y(x,t)}{\sqrt{\mu(x)}}\right). \tag{27}$$

Note that in 1D, the divergence of $H_y(x,t)$ and $E_z(x,t)$ is zero. Hence, Eqs. (3) and (4) are automatically satisfied.

Using the second-order central-difference approximation to the first derivative with respect to x, we obtain

$$\frac{\partial}{\partial t}X_y(i,t) = \frac{1}{\delta\sqrt{\mu_i}}\left(\frac{Y_z(i+1,t)}{\sqrt{\varepsilon_{i+1}}} - \frac{Y_z(i-1,t)}{\sqrt{\varepsilon_{i-1}}}\right), \tag{28}$$

$$\frac{\partial}{\partial t}Y_z(j,t) = \frac{1}{\delta\sqrt{\varepsilon_j}}\left(\frac{X_y(j+1,t)}{\sqrt{\mu_{j+1}}} - \frac{X_y(j-1,t)}{\sqrt{\mu_{j-1}}}\right), \tag{29}$$

where the integer i labels the grid points and δ denotes the distance between two next-nearest neighbor lattice points (hence, the absence of a factor two in the nominator). For notational simplicity we will, from now on, specify the spatial coordinates through the lattice index i, e.g., $X_y(i,t)$ stands for $X_y(x=(i+1)\delta/2,t)$.

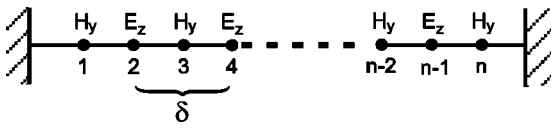

FIG. 1. Positions of the two TM-mode field components on the one-dimensional grid.

Following Yee [2], it is convenient to assign $X_y(i,t)$ and $Y_z(j,t)$ to the odd and even-numbered lattice site, respectively, as shown in Fig. 1 for a grid of n points. The Eqs. (28) and (29) may now be combined into one equation of the form Eq. (8) by introducing the n-dimensional vector

$$\Psi(i,t) = \begin{cases} X_y(i,t) = \sqrt{\mu_i}H_y(i,t), & i \text{ odd} \\ Y_z(i,t) = \sqrt{\varepsilon_i}E_z(i,t), & i \text{ even} \end{cases}. \tag{30}$$

The vector $\Psi(t)$ describes both the magnetic and the electric field on the lattice points $i=1,\ldots,n$. As usual, the ith element of $\Psi(t)$ is given by the inner product $\Psi(i,t) = \mathbf{e}_i^T\cdot\Psi(t)$ where $\mathbf{e}_i$ denotes the ith unit vector in the n-dimensional vector space. Using this notation, it is easy to show that Eqs. (28) and (29) reduce to

$$\frac{\partial}{\partial t}\Psi(t) = H\Psi(t), \tag{31}$$

where the matrix H is given by

$$H = \sum_{i=1}{}' [\beta_{i+1,i}(\mathbf{e}_i\mathbf{e}_{i+1}^T - \mathbf{e}_{i+1}\mathbf{e}_i^T) + \beta_{i+1,i+2}(\mathbf{e}_{i+1}\mathbf{e}_{i+2}^T - \mathbf{e}_{i+2}\mathbf{e}_{i+1}^T)], \tag{32}$$

with $\beta_{i,j} = 1/(\delta\sqrt{\varepsilon_i\mu_j})$ and the prime indicates that the sum is over odd integers only. In complete analogy to Eq. (10), the time evolution of $\Psi(t)$ is formally given by $\Psi(t) = U(t)\Psi(0)$ with $U(t) = \exp(tH)$.

The notation introduced above will prove most useful for the cases of 2D and 3D for which it is rather cumbersome to write down matrix representations. For the 1D case, it is not difficult and in fact very instructive to write down the matrix H explicitly. Indeed, we have

$$H = \begin{pmatrix} 0 & \beta_{2,1} & & & & \\ -\beta_{2,1} & 0 & \beta_{2,3} & & & \\ & \ddots & \ddots & \ddots & & \\ & & -\beta_{n-1,n-2} & 0 & \beta_{n-1,n} & \\ & & & -\beta_{n-1,n} & 0 & \end{pmatrix}, \tag{33}$$

and we immediately see that H is skew symmetric by construction. Furthermore, for n odd we have

$$\frac{\partial}{\partial t}\Psi(1,t)=\beta_{2,1}\Psi(2,t) \quad \text{and} \quad \frac{\partial}{\partial t}\Psi(n,t) = -\beta_{n-1,n}\Psi(n-1,t), \tag{34}$$

such that the electric field vanishes at the boundaries $[Y_z(0,t)=Y_z(n+1,t)=0$, see also Fig. 1], as required by the boundary conditions Eq. (5). For this reason, we only consider the case of n odd in the sequel.

According to the general procedure outlined in Sec. III, the final step in the construction of an unconditionally stable algorithm is to decompose H. Guided by previous work on Schrödinger and diffusion problems [17,19,24,25], we split H into two parts, i.e., $H=H_1+H_2$, where

$$H_1=\sum_{i=1}^{n}{}'\beta_{i+1,i}(\mathbf{e}_i\mathbf{e}_{i+1}^T-\mathbf{e}_{i+1}\mathbf{e}_i^T), \tag{35}$$

$$H_2=\sum_{i=1}^{n}{}'\beta_{i+1,i+2}(\mathbf{e}_{i+1}\mathbf{e}_{i+2}^T-\mathbf{e}_{i+2}\mathbf{e}_{i+1}^T), \tag{36}$$

i.e., we divide the lattice into odd- and even-numbered cells. In matrix notation, we have

$$H_1=\begin{pmatrix} 0 & \beta_{2,1} & & & & & & & \\ -\beta_{2,1} & 0 & 0 & & & & & & \\ & 0 & 0 & \beta_{4,3} & & & & & \\ & & -\beta_{4,3} & 0 & 0 & & & & \\ & & & 0 & \ddots & 0 & & & \\ & & & & 0 & 0 & \beta_{n-1,n-2} & & \\ & & & & & -\beta_{n-1,n-2} & 0 & 0 & \\ & & & & & & 0 & 0 & \end{pmatrix} \tag{37}$$

and

$$H_2=\begin{pmatrix} 0 & 0 & & & & & & & \\ 0 & 0 & \beta_{2,3} & & & & & & \\ & -\beta_{2,3} & 0 & 0 & & & & & \\ & & 0 & \ddots & 0 & & & & \\ & & & 0 & 0 & \beta_{n-3,n-2} & & & \\ & & & & -\beta_{n-3,n-2} & 0 & 0 & & \\ & & & & & 0 & 0 & \beta_{n-1,n} & \\ & & & & & & -\beta_{n-1,n} & 0 & \end{pmatrix}. \tag{38}$$

Clearly, both H_1 and H_2 are skew-symmetric block-diagonal matrices, containing one 1×1 matrix and $(n-1)/2$ real, 2×2 skew-symmetric matrices.

According to the general theory given above, the first-order algorithm defined by

$$U_1(\tau)=e^{\tau H_1}e^{\tau H_2} \tag{39}$$

is all that is needed to construct unconditionally stable second- and higher-order algorithms. As the matrix exponential of a block-diagonal matrix is equal to the block-diagonal matrix of the matrix exponentials of the individual blocks, the numerical calculation of $e^{\tau H_1}$ (or $e^{\tau H_2}$) reduces to the calculation of $(n-1)/2$ matrix exponentials of 2×2 matrices. The matrix exponential of a typical 2×2 matrix appearing in $e^{\tau H_1}$ or $e^{\tau H_2}$ is given by

$$\exp\left[\alpha\begin{pmatrix} 0 & 1 \\ -1 & 0 \end{pmatrix}\right]\begin{pmatrix} \Psi(i,t) \\ \Psi(j,t) \end{pmatrix}=\begin{pmatrix} \cos\alpha & \sin\alpha \\ -\sin\alpha & \cos\alpha \end{pmatrix}\begin{pmatrix} \Psi(i,t) \\ \Psi(j,t) \end{pmatrix}. \tag{40}$$

B. Two dimensions

Assuming translational invariance with respect to the z direction, the system effectively becomes 2D and the TDME separate into two sets of equations [1]. For conciseness, in this section we only discuss the set of equations for the TM modes. The TE modes may be treated in exactly the same manner.

The relevant EM fields for the TM modes in 2D are $\Psi(t)=[\mathbf{X}_x(x,y,t),\mathbf{X}_y(x,y,t),\mathbf{Y}_z(x,y,t)]^T$, in terms of which TDME Eq. (7) reads

$$\frac{\partial}{\partial t}\Psi(t)=\mathcal{H}\Psi(t)=\begin{pmatrix} 0 & 0 & -\frac{1}{\sqrt{\mu}}\frac{\partial}{\partial y}\frac{1}{\sqrt{\varepsilon}} \\ 0 & 0 & \frac{1}{\sqrt{\mu}}\frac{\partial}{\partial x}\frac{1}{\sqrt{\varepsilon}} \\ -\frac{1}{\sqrt{\varepsilon}}\frac{\partial}{\partial y}\frac{1}{\sqrt{\mu}} & \frac{1}{\sqrt{\varepsilon}}\frac{\partial}{\partial x}\frac{1}{\sqrt{\mu}} & 0 \end{pmatrix}\Psi(t). \tag{41}$$

We discretize continuum space by simply reusing the one-dimensional lattice introduced above, as exemplified in Fig. 2 for the case of the TM modes. This construction automatically takes care of the boundary conditions if n_x and n_y are odd and yields a real skew-symmetric matrix H.

In analogy with the 1D case, the elements of $\Psi(t)$ are defined by

$$\Psi(i,j,t) = \begin{cases} Y_z(i,j,t)=\sqrt{\varepsilon_{i,j}}E_z(i,j,t), & i \text{ even and } j \text{ even} \\ X_y(i,j,t)=\sqrt{\mu_{i,j}}H_y(i,j,t), & i \text{ odd and } j \text{ even} \\ X_x(i,j,t)=\sqrt{\mu_{i,j}}H_x(i,j,t), & i \text{ even and } j \text{ odd} \end{cases}. \tag{42}$$

Discretization of the differential operators that appear in Eq. (41) yield expressions that have the same structure as Eq. (33), with extra subscripts to account for the second spatial dimension. It follows that on the lattice,

$$\frac{\partial}{\partial t}\Psi(t)=H\Psi(t) = \sum_{i=1}^{n_x}{}'\sum_{j=1}^{n_y}{}'[H^{(x)}(i,j)+H^{(y)}(i,j)]\Psi(t), \tag{43}$$

where

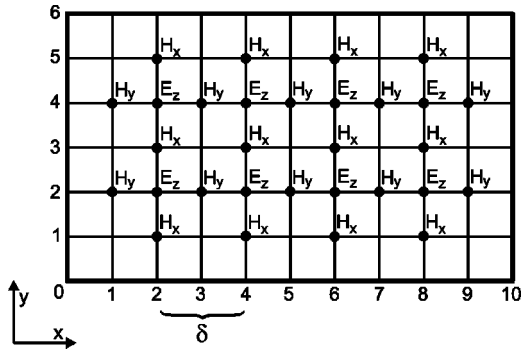

FIG. 2. Positions of the three TM-mode EM-field components on the two-dimensional grid for $n_x=9$ and $n_y=5$.

$$H^{(x)}(i,j)=+\frac{\mathbf{e}_{i,j+1}\mathbf{e}_{i+1,j+1}^T-\mathbf{e}_{i+1,j+1}\mathbf{e}_{i,j+1}^T}{\delta\sqrt{\varepsilon_{i+1,j+1}\mu_{i,j+1}}} + \frac{\mathbf{e}_{i+1,j+1}\mathbf{e}_{i+2,j+1}^T-\mathbf{e}_{i+2,j+1}\mathbf{e}_{i+1,j+1}^T}{\delta\sqrt{\varepsilon_{i+2,j+1}\mu_{i+2,j+1}}}, \tag{44}$$

$$H^{(y)}(i,j)=-\frac{\mathbf{e}_{i+1,j}\mathbf{e}_{i+1,j+1}^T-\mathbf{e}_{i+1,j+1}\mathbf{e}_{i+1,j}^T}{\delta\sqrt{\varepsilon_{i+1,j+1}\mu_{i+1,j}}} - \frac{\mathbf{e}_{i+1,j+1}\mathbf{e}_{i+1,j+2}^T-\mathbf{e}_{i+1,j+2}\mathbf{e}_{i+1,j+1}^T}{\delta\sqrt{\varepsilon_{i+1,j+2}\mu_{i+1,j+1}}}, \tag{45}$$

and the superscripts (x) and (y) refer to the derivative with respect to x and y, respectively. Note that we use the pair (i,j) to label the n_xn_y unit vectors $\mathbf{e}_{i,j}$. In complete analogy with the 1D, case we split Eqs. (44) and (45) into two parts and obtain for the first-order approximation to $U(\tau)$

$$U_1(\tau)=e^{\tau H_1^{(x)}}e^{\tau H_2^{(x)}}e^{\tau H_1^{(y)}}e^{\tau H_2^{(y)}}, \tag{46}$$

where for instance, in formal analogy to Eq. (36), we have

$$H_2^{(x)}=\sum_{i=1}^{n_x}{}'\sum_{j=1}^{n_y}{}'\frac{\mathbf{e}_{i+1,j+1}\mathbf{e}_{i+2,j+1}^T-\mathbf{e}_{i+2,j+1}\mathbf{e}_{i+1,j+1}^T}{\delta\sqrt{\varepsilon_{i+2,j+1}\mu_{i+2,j+1}}}. \tag{47}$$

It is not difficult to convince oneself that approximation $U_1(\tau)$ and hence also $U_2(\tau)$ and $U_4(\tau)$ do not commute with the (lattice version of) the divergence. Therefore, the divergence of the EM fields in 2D is not conserved. Although the initial state (at $t=0$) of the EM fields satifies Eqs. (3) and (4), time-integration of the TDME using $U_k(\tau)$ yields a solution that will not satisfy Eqs. (3) and (4). However, for algorithm $U_k(\tau)$, the deviations from zero vanish as τ^k so that in practice these errors are under control and may be made sufficiently small for practical purposes.

C. Three dimensions

In terms of $\Psi(t)=(\mathbf{X}(t),\mathbf{Y}(t))^T$ for a 3D system, Eq. (7) reads

$$\frac{\partial}{\partial t}\Psi(t)=\mathcal{H}\Psi(t)=\begin{pmatrix} 0 & h \\ -h^T & 0 \end{pmatrix}\Psi(t), \tag{48}$$

where h is given by

$$h=\begin{pmatrix} 0 & \frac{1}{\sqrt{\mu}}\frac{\partial}{\partial z}\frac{1}{\sqrt{\varepsilon}} & -\frac{1}{\sqrt{\mu}}\frac{\partial}{\partial y}\frac{1}{\sqrt{\varepsilon}} \\ -\frac{1}{\sqrt{\mu}}\frac{\partial}{\partial z}\frac{1}{\sqrt{\varepsilon}} & 0 & \frac{1}{\sqrt{\mu}}\frac{\partial}{\partial x}\frac{1}{\sqrt{\varepsilon}} \\ \frac{1}{\sqrt{\mu}}\frac{\partial}{\partial y}\frac{1}{\sqrt{\varepsilon}} & -\frac{1}{\sqrt{\mu}}\frac{\partial}{\partial x}\frac{1}{\sqrt{\varepsilon}} & 0 \end{pmatrix}. \tag{49}$$

We discretize the spatial coordinates by adopting the standard Yee grid [2]. We show a unit cell of this grid in Fig. 3. In analogy to the systems in 1D and 2D, we assign the EM fields to the lattice points such that the boundary conditions Eq. (5) are automatically satisfied. The elements of the vector $\Psi(i,j,k,t)$ are given by

$$\Psi(i,j,k,t)=\begin{cases} X_x(i,j,k,t)=\sqrt{\mu_{i,j,k}}H_x(i,j,k,t), & i \text{ even, } j \text{ odd, } k \text{ odd} \\ X_y(i,j,k,t)=\sqrt{\mu_{i,j,k}}H_y(i,j,k,t), & i \text{ odd, } j \text{ even, } k \text{ odd} \\ X_z(i,j,k,t)=\sqrt{\mu_{i,j,k}}H_z(i,j,k,t), & i \text{ odd, } j \text{ odd, } k \text{ even} \\ Y_x(i,j,k,t)=\sqrt{\varepsilon_{i,j,k}}E_x(i,j,k,t), & i \text{ odd, } j \text{ even, } k \text{ even} \\ Y_y(i,j,k,t)=\sqrt{\varepsilon_{i,j,k}}E_y(i,j,k,t), & i \text{ even, } j \text{ odd, } k \text{ even} \\ Y_z(i,j,k,t)=\sqrt{\varepsilon_{i,j,k}}E_z(i,j,k,t), & i \text{ even, } j \text{ even, } k \text{ odd} \end{cases}, \tag{50}$$

for the origin of the coordinate system $(i,j,k)=(0,0,0)$ at the center of the unit cell shown in Fig. 3. The number of lattice points in the x, y, and z direction will be denoted by n_x, n_y, and n_z respectively. As before, these numbers are assumed to be odd.

Discretization of the differential operators that appear in Eq. (49) yields Eq. (7) in the form

$$\frac{\partial}{\partial t}\Psi(t)=H\Psi(t)=\sum_{i=1}^{n_x}{}'\sum_{j=1}^{n_y}{}'\sum_{k=1}^{n_z}{}'[H^{(x)}(i,j,k)+H^{(y)}(i,j,k)+H^{(z)}(i,j,k)]\Psi(t), \tag{51}$$

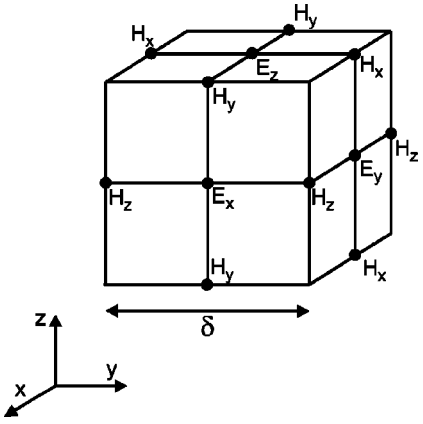

FIG. 3. Unit cell of the Yee grid.

where the superscripts (x), (y), and (z) refer to the derivative with respect to x, y, and z, respectively,

$$\begin{aligned} H^{(x)}(i,j,k)=&+\frac{\mathbf{e}_{i,j+1,k}\mathbf{e}_{i+1,j+1,k}^T-\mathbf{e}_{i+1,j+1,k}\mathbf{e}_{i,j+1,k}^T}{\delta\sqrt{\varepsilon_{i+1,j+1,k}\mu_{i,j+1,k}}} \\ &-\frac{\mathbf{e}_{i,j,k+1}\mathbf{e}_{i+1,j,k+1}^T-\mathbf{e}_{i+1,j,k+1}\mathbf{e}_{i,j,k+1}^T}{\delta\sqrt{\varepsilon_{i+1,j,k+1}\mu_{i,j,k+1}}} \\ &+\frac{\mathbf{e}_{i+1,j+1,k}\mathbf{e}_{i+2,j+1,k}^T-\mathbf{e}_{i+2,j+1,k}\mathbf{e}_{i+1,j+1,k}^T}{\delta\sqrt{\varepsilon_{i+1,j+1,k}\mu_{i+2,j+1,k}}} \\ &-\frac{\mathbf{e}_{i+1,j,k+1}\mathbf{e}_{i+2,j,k+1}^T-\mathbf{e}_{i+2,j,k+1}\mathbf{e}_{i+1,j,k+1}^T}{\delta\sqrt{\varepsilon_{i+1,j,k+1}\mu_{i+2,j,k+1}}}, \end{aligned} \tag{52}$$

and the expressions for $H^{(y)}(i,j,k)$ and $H^{(z)}(i,j,k)$ follow from Eq. (52) by symmetry. Note that we use the triple (i,j,k) to label the $n_xn_yn_z$ unit vectors $\mathbf{e}_{i,j,k}$.

In complete analogy with the 1D and 2D cases, we split Eq. (52) [as well as $H^{(y)}(i,j,k)$ and $H^{(z)}(i,j,k)$] into two parts and obtain for the first-order approximation to $U(\tau)$

$$U_1(\tau)=e^{\tau H_1^{(x)}}e^{\tau H_2^{(x)}}e^{\tau H_1^{(y)}}e^{\tau H_2^{(y)}}e^{\tau H_1^{(z)}}e^{\tau H_2^{(z)}}, \tag{53}$$

where, for instance,

$$H_1^{(z)}=\sum_{i=1}^{n_x}{}'\sum_{j=1}^{n_y}{}'\sum_{k=1}^{n_z}{}'\left(\frac{\mathbf{e}_{i,j+1,k}\mathbf{e}_{i,j+1,k+1}^T-\mathbf{e}_{i,j+1,k+1}\mathbf{e}_{i,j+1,k}^T}{\delta\sqrt{\varepsilon_{i,j+1,k+1}\mu_{i,j+1,k}}}-\frac{\mathbf{e}_{i+1,j,k}\mathbf{e}_{i+1,j,k+1}^T-\mathbf{e}_{i+1,j,k+1}\mathbf{e}_{i+1,j,k}^T}{\delta\sqrt{\varepsilon_{i+1,j,k+1}\mu_{i+1,j,k}}}\right). \tag{54}$$

Note that each contribution to Eq. (54) acts on a different pair of elements of $\Psi(t)$. Hence, each of the matrix exponentials in Eq. (53) acts on one quarter of all the lattice points. Performing the time-step operation, Eq. (53) involves only two sweeps over all lattice points.

By construction, the algorithm defined by Eq. (53) is unconditionally stable and so are the higher-order algorithms defined by $U_2(\tau)$ and $U_4(\tau)$. Each contribution to, e.g., Eq. (54) is of the form Eq. (35) and hence its matrix exponential may be calculated in exactly the same manner as in the 1D case [see Eq. (40)]. The divergence of the EM fields in 3D is, for the same reason as in the 2D case, not conserved but decreases as τ^k.

D. Implementation: Summary

The notation required to write down the algorithms in mathematical form might give the impression that these algorithms are difficult to program. Actually, that is not the case, on the contrary. Recall that the first-order algorithm $U_1(\tau)$ is all we need to program: As explained in Sec. III, more accurate schemes may be implemented without extra programming. Let us consider the algorithm for the case of 1D. For 2D and 3D, we simply repeat the steps described below two, and three times, respectively. We have

$$U_1(\tau)=e^{\tau H_1}e^{\tau H_2}=\left\{\prod_{i=1}^{n}{}'\exp[\beta_{i+1,i}(\mathbf{e}_i\mathbf{e}_{i+1}^T-\mathbf{e}_{i+1}\mathbf{e}_i^T)]\right\}\times\left\{\prod_{i=1}^{n}{}'\exp[\beta_{i+1,i+2}(\mathbf{e}_{i+1}\mathbf{e}_{i+2}^T-\mathbf{e}_{i+2}\mathbf{e}_{i+1}^T)]\right\}, \tag{55}$$

where we used the block-diagonal structure of H_1 and H_2 (see Eqs. (37) and (38)) to obtain an exact expression for $U_1(\tau)$ in terms of an ordered product of matrix exponentials. Each of these matrix exponentials only operates on a pair of elements of $\Psi(t)$ and leaves other elements intact. The indices of each of these pairs are given by the subscripts of $\mathbf{e}$ and $\mathbf{e}^T$. From Eq. (55), it is then clear what the program should do: Make loops over i with stride two. For each i, pick a pair of elements from $\Psi(t)$ according to the subscripts of $\mathbf{e}$ and $\mathbf{e}^T$, compute (or recall from memory) the elements of the plane rotation [see Eq. (40)], perform the plane rotation, i.e., multiply the 2×2 matrices and the vectors of length two, and overwrite the same two elements.

It also follows immediately that performing a time step with algorithms based on Eq. (55) takes $O(K)$ plane rotations where K is the total number of elements of the vector $\Psi(t)$ (which is less or equal to the number of grid points). This renders the algorithm efficient: The number of operations to complete one time step scales linearly with the number of grid points. Also, note that there is a high degree of intrinsic parallelism in this class of algorithms. In principle, the $(n-1)/2$ matrix-vector multiplications that implement $e^{\tau H_1}$ or $e^{\tau H_2}$ may be done in parallel.

In the absence of external currents (see below), updating the EM field values of a 3D system using the the Yee algorithm requires six arithmetic operations [see Eq. (33) in Ref. [3]] whereas the second-order algorithm $U_2(\tau)$ requires 33 arithmetic operations. For 1D and 2D problems, the ratio is 9/4 and 21/6, respectively. Thus, in terms of CPU time, the price paid for the unconditional stability of the algorithms is not that much and for some applications (see below) may well be worth paying.

An important aspect that we have not yet discussed is the effect of the discretization of space on the accuracy of the numerical results. Both conditional Yee-type algorithms and unconditionally stable algorithms $U_1(\tau)$, $U_2(\tau)$, and $U_4(\tau)$ suffer from numerical dispersion (see Ref. [3], Chap. 4, for an in-depth discussion). Simple methods to reduce numerical dispersion are taking a finer mesh or employing more accurate finite-difference approximations for the spatial derivates [3]. The former obviously may be used here too (for the simulations discussed below, we used a mesh size that yields sufficiently accurate results for the present purposes). There are no fundamental nor practical problems to incorporate the latter method in the Suzuki-product-formula approach [17,19]. However, as the emphasis of the present paper is on the construction of unconditionally stable algorithms, we relegate a presentation of these technical, but for applications, important extensions to future publications.

V. DATA ANALYSIS

Time-domain algorithms obviously yield the time development of the EM fields. The scattering (transmission) of the EM fields from (through) objects is one of the main applications of this technique [3]. One approach is to prepare an initial state $\Psi(0)$ of the EM fields, propagate the fields in time for a number of time steps, and analyze the scattered and/or transmitted fields. Another, more realistic, approach is to use a current source $\mathbf{J}(t)=\mathbf{J}(\mathbf{r},t)$. Instead of Eq. (8), we have

$$\frac{\partial}{\partial t}\Psi(t)=\mathcal{H}\Psi(t)-\mathcal{J}(t), \tag{56}$$

where $\Psi(t)=[\mathbf{X}(t),\mathbf{Y}(t)]^T$ and $\mathcal{J}(t)=[0,\mathbf{J}(t)]^T$ represents the source term. The formal solution of Eq. (56) is given by

$$\Psi(t)=e^{t\mathcal{H}}\Psi(0)-\int_0^t e^{(t-u)\mathcal{H}}\mathcal{J}(u)du, \tag{57}$$

showing that we may simply reuse one of the unconditionally stable algorithms to compute the second term in Eq. (57). In practice, for a time-step τ, we update $\Psi(t)$ according to

$$\Psi(t+\tau)=e^{\tau\mathcal{H}}\Psi(t)-\int_t^{t+\tau}e^{(t+\tau-u)\mathcal{H}}\mathcal{J}(u)du. \quad (58)$$

A standard quadrature formula may be used to compute the integral over u [24]. When a current source is present, we take as the initial condition $\Psi(0)=0$.

Time-domain algorithms may also be used to compute the eigenvalues of H, the discretized form of $\mathcal{H}$. In general, H is a (very) large matrix, usually too large to be stored in memory. If only a few, well-separated eigenvalues of H are required, sparse-matrix techniques can be used to compute these eigenvalues [12,27]. However, if one is interested in global features of the distribution of eigenvalues, i.e., if we want to determine *all* eigenvalues, time-domain algorithms offer several advantages. In fact, they are at the heart of so-called ''fast'' algorithms to compute the density of states (DOS) and other related quantities [28–33]. The basic idea of this approach was laid out by Alben *et al.* [28] who used it to compute the DOS of models for one electron moving in a disordered alloy.

Denoting the (unknown) eigenvalues and (unknown) eigenvectors of H by iE_j and ϕ_j, respectively, we have

$$f(t)\equiv\frac{\langle\Psi(0)|\Psi(t)\rangle}{\langle\Psi(0)|\Psi(0)\rangle}=\frac{\langle\Psi(0)|e^{tH}\Psi(0)\rangle}{\langle\Psi(0)|\Psi(0)\rangle}$$
$$=\sum_{i=1}^{K}e^{itE_i}\frac{\langle\Psi(0)|\phi_i\rangle|^2}{\langle\Psi(0)|\Psi(0)\rangle}, \quad (59)$$

where K ($K=n$ for 1D, $K=3n_xn_y/4$ for 2D, $K=3n_xn_yn_z/4$ for 3D) is the dimension of the vector space on which H acts. From Eq. (59), it follows immediately that the Fourier transform of $f(t)$ contains the information on all eigenvalues for which $|\langle\Psi(0)|\phi_i\rangle|>0$. Using independent random numbers to initialize the elements of $\Psi(0)$, it may be shown that the density of states $\mathcal{D}(\omega)$ is given by [26]

$$\mathcal{D}(\omega)=a\int_{-\infty}^{+\infty}e^{-i\omega t}\overline{f(t)}dt, \quad (60)$$

where a is an irrelevant constant factor and $\overline{f(t)}$ is the average of $f(t)$ over different realizations of the random initial state. It is often expedient to consider, in addition to $\mathcal{D}(\omega)$, the integrated density of states

$$N(\omega)=\int_{-\infty}^{\omega}\mathcal{D}(u)du. \quad (61)$$

The statistical error on $f(t)$ vanishes as $1/\sqrt{SK}$ where S is the number of statistically independent samples of $\Psi(0)$ [26]. The fact that the statistical error decreases with the number of lattice points $K/2$ gives a tremendous boost to the efficiency of the method.

The information on the eigenvalues of H, obtained through the use of a time-domain method is intimately related to the unconditional stability of the latter. As $f(t)$ is band-limited, with frequencies E_j in the interval $[-\|H\|,\|H\|]$ (where $\|H\|$ denotes the largest eigenvalue of H in absolute value), it follows from Nyquist's sampling theorem that it is sufficient to sample $f(t)$ at regular intervals $\Delta t=\pi/\|H\|$. If N denotes the number of data points used to sample $f(t)$, frequencies E_j that differ less than $\Delta E=\pi/N\Delta t$ are indistinguishable (although they will all contribute to the DOS). Extending the length of the time integration by a factor of two increases the resolution in frequency by a factor of two. This is a rather efficient and flexible procedure to trade accuracy for computational resources. One may object that by integrating the TDME over longer and longer times (larger and larger N) the error on $\Psi(t)$ will increase, possibly leading to no gain in accuracy at all. However, it has been shown rigorously [26] that the error on the eigenvalues of H vanishes as τ^2/N if one uses unconditionally stable algorithms based on the second-order Suzuki product formula. The proof given in Ref. [26] applies to the fourth-order algorithm $U_4(\tau)$ as well, the exponent of τ being four instead of two.

In some cases, the underlying differential equations and boundary conditions only specify the solution up to a nonzero constant. In the calculation of the DOS, the presence of such a constant contribution shows up as a peak at zero frequency. In principle, this peak may be removed by modifying the random initial state but as the origin of this irrelevant artifact is understood, there is little reason for doing this.

To summarize, solving the TDME by the kth-order Suzuki product-formula algorithm $U_k(\tau)$ guarantees that the accuracy with which the eigenvalues of H may be determined vanishes as τ^k/N, where N is the number of points used to sample $f(t)$ [see Eq. (59)].

VI. SIMULATION RESULTS

In this section, we present simulation results for several physical systems that we selected as examples to test our algorithms. For numerical purposes, it is expedient to use dimensionless quantities. We will denote the unit of length by λ and take the velocity of light in vacuum c as the unit of velocity. Then time and frequency are measured in units of λ/c and c/λ, respectively. The permittivity ε and permeability μ are measured in units of their corresponding values in vacuum.

A. One dimension

Let us first consider an empty, one-dimensional cavity with constant permeability $\mu=1$ and constant permittivity $\varepsilon=1$. The eigenfrequencies for a system of length L are given by [1]

$$\omega_k=\frac{\pi k}{L}, \quad (62)$$

where $k=0,1,2,\ldots,$ labels the different EM modes. In Fig. 4, we show the density of states $|\mathcal{D}(\omega)|$ obtained according

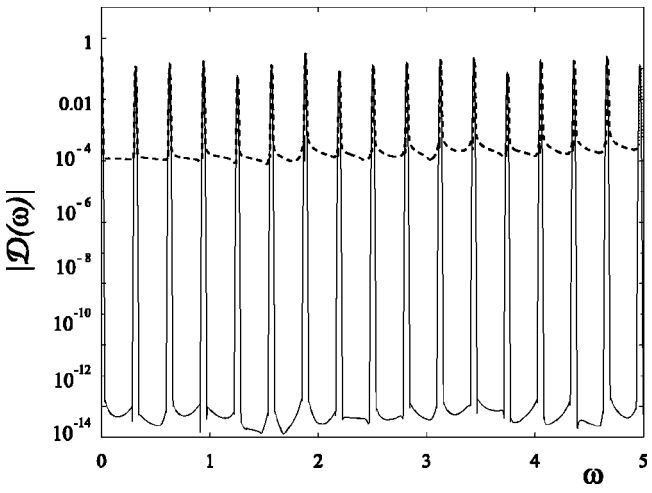

FIG. 4. Density of states of a one-dimensional cavity of length $L=10$. Solid line: $U_2(\tau)$ algorithm; dashed line: standard Yee algorithm.

to the procedure described in Sec. V, using the second-order algorithm $U_2(\tau)$ (solid line) and the standard Yee algorithm [2,3] (dashed line). In both calculations, the lattice spacing $\delta=0.1$ and the time step $\tau=0.01$. Each curve shown in Fig. 4 is the average of $S=10$ statistically independent runs, taking $N=16\,384$ samples of $f(t)$ [see Eq. (59)] at time intervals $\Delta t=0.1$. The peaks in Fig. 4 correspond to the exact frequencies [see Eq. (62)] of the 1D cavity. The background signal produced by the Yee algorithm [2,3] is at least eight orders of magnitude larger than that generated by $U_2(\tau)$. The time step operator of the Yee algorithm is not an orthogonal matrix and hence its eigenvalues do not necessarily lie on the unit circle. This is related to the fact that the Yee algorithm is conditionally stable [3] and leads to fluctuations in the energy density $w(t)$, as illustrated by the dashed line in Fig. 5, and to negative values of the Fourier transform of $f(t)$ [which is the reason why Fig. 4 shows $|\mathcal{D}(\omega)|$ instead of $\mathcal{D}(\omega)$].

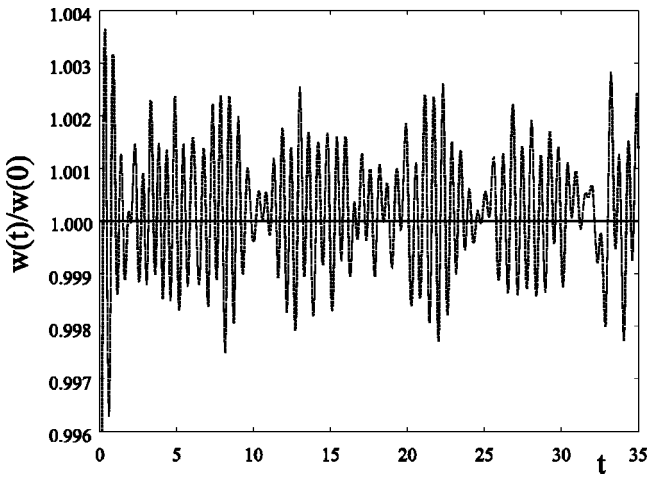

FIG. 5. Normalized total energy density as a function of time for the same physical system as in Fig. 4. Solid line: $U_2(\tau)$; dashed line: standard Yee algorithm.

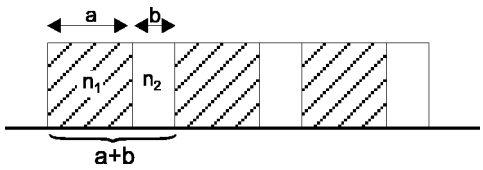

FIG. 6. Structure of a one-dimensional stack of dielectric material.

In contrast, the unconditional stability of algorithms based on the Suzuki product formula implies that $w(t)$ is constant in time. The solid line in Fig. 5 shows that this is indeed the case.

As a second example, we consider a one-dimensional stack of dielectric material, schematically shown in Fig. 6. The material indices of refraction, denoted by n_1 and n_2, give rise to a spatially varying permittivity

$$\varepsilon(x)=\begin{cases} n_1^2, & \text{if } x \bmod(a+b)\leqslant a \\ n_2^2, & \text{if } x \bmod(a+b)>a \end{cases}. \tag{63}$$

In particular, we consider a structure that is known as the quarter-wave stack and is characterized by the relation

$$n_1 a = n_2 b, \tag{64}$$

such that the length of the optical path in the two layers is the same. The density of states exhibits a gap centered around the midgap frequency [1,34]

$$\omega_0=\frac{\pi}{2n_1 a}. \tag{65}$$

In Fig. 7, we show the density of states $\mathcal{D}(\omega)$ as obtained by $U_2(\tau)$.

Also for these calculations, the lattice spacing $\delta=0.1$ and the time step $\tau=0.01$. Each curve in Fig. 7 is the average of $S=100$ statistically independent runs, taking $N=16\,384$

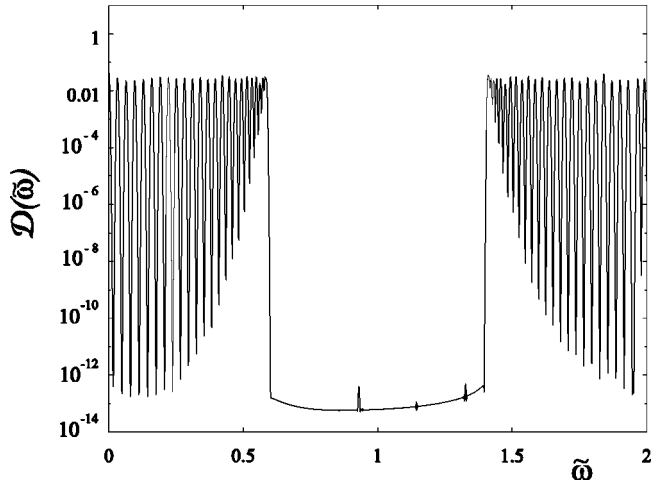

FIG. 7. Density of states, as obtained by the $U_2(\tau)$ algorithm, of a quarter-wave stack of length $L=24.9$ and with parameters $n_1=1$, $n_2=4$, $a=0.8$, $b=0.2$ (see Fig. 6) as a function of the rescaled frequency $\tilde{\omega}=\omega/\omega_0$.

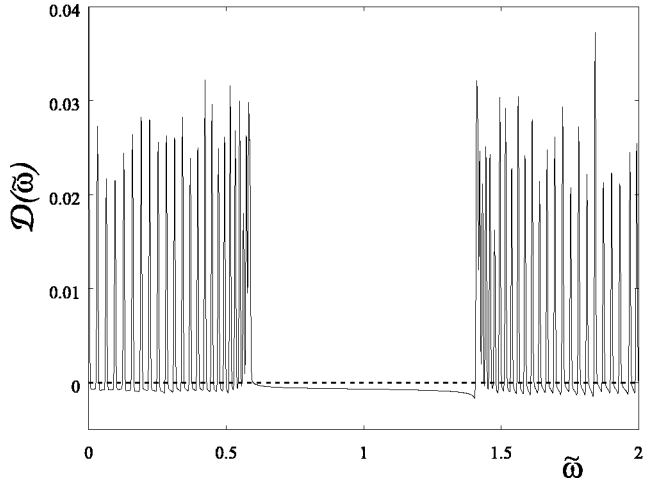

FIG. 8. Density of states, as obtained by the standard Yee algorithm, of a quarter-wave stack of length $L=24.9$ and with parameters $n_1=1$, $n_2=4$, $a=0.8$, $b=0.2$ (see Fig. 6) as a function of the rescaled frequency $\tilde{\omega}=\omega/\omega_0$. Note the difference in the vertical scale between Figs. 7 and 8.

samples of $f(t)$ [see Eq. (59)] at time intervals $\Delta t=0.1$. Note that the system length L and the (odd) number of lattice points have to be chosen judisciously, otherwise the spectrum will exhibit artifacts (impurity states due to one extra grid point).

In Fig. 8, we show the density of states $\mathcal{D}(\omega)$ as obtained by the Yee algorithm. Note that the spectral weight may take negative values, an unphysical feature that is a manifestation of the fact that the energy of the EM field is not conserved.

In Fig. 9, we present the integrated density of states $N(\omega)$ for both the $U_2(\tau)$ and Yee algorithm. The result of the $U_2(\tau)$ algorithm is in excellent agreement with the analytical calculation [34].

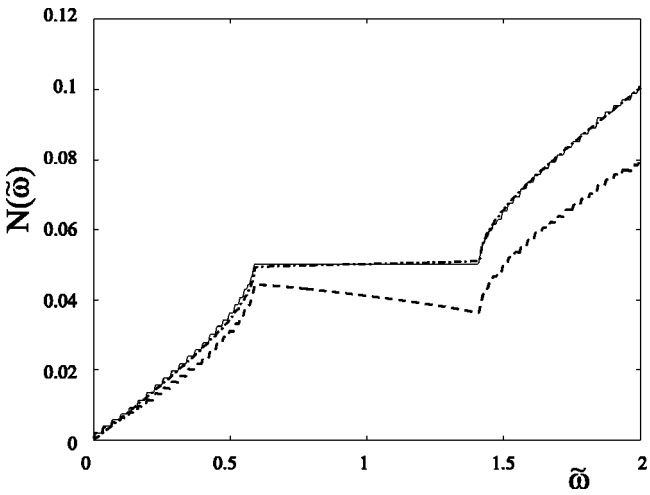

FIG. 9. Integrated density of states as function of the rescaled frequency $\tilde{\omega}=\omega/\omega_0$, for the same system as in Figs. 7 and 8. Solid line: $U_2(\tau)$ algorithm; dashed line: standard Yee algorithm; dashed-dotted line: analytical result.

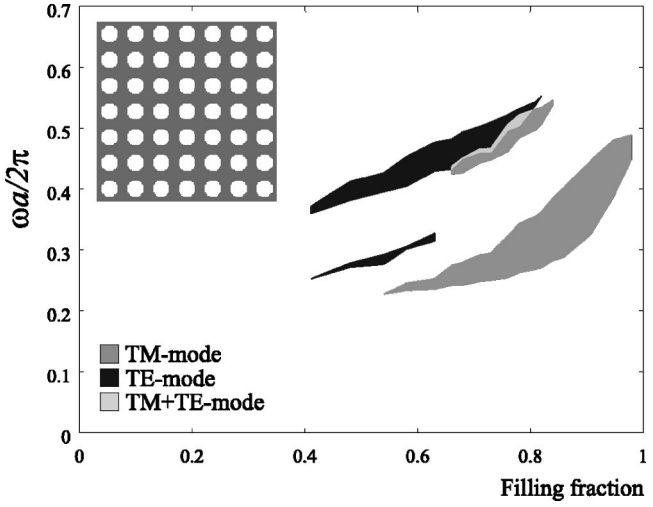

FIG. 10. Absolute photonic band gaps of a dielectric material ($\varepsilon=11.4$) pierced by air-filled cylinders. The largest overlap of the TM- and TE-mode gaps occurs at a filling fraction of approximately 0.77.

B. Two dimensions

A photonic band gap (PBG) material prohibits the propagation of EM fields in a range of frequencies that is characteristic for its structure [35]. A PBG is called absolute if it exists for any wave vector of the EM fields. The most common method used to compute a PBG employs a plane-wave expansion to solve the time-independent Maxwell equations (see, e.g., [36]). This kind of PBG calculation requires a Fourier transform of the unit cell of the dielectric structure that is for simplicity considered to be periodic.

With our time-domain algorithm, the existence of a PBG may be demonstrated with relative ease. It suffices to compute the spectrum of such a dielectric structure with a random initial state. If the spectrum is gapless there is no need to make additional runs. If there is a signature of a gap, it

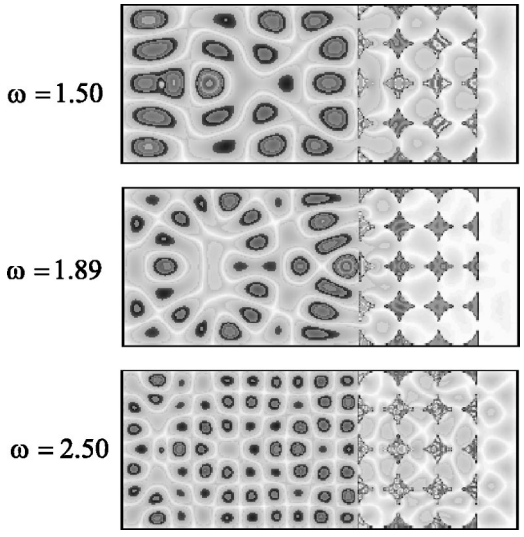

FIG. 11. Snapshot of the intensity E_z^2 at $t=102.4$. Dimensions of the system: 30×12.1; point source located at (6,6) (see Fig. 2), emitting radiation with frequency ω.

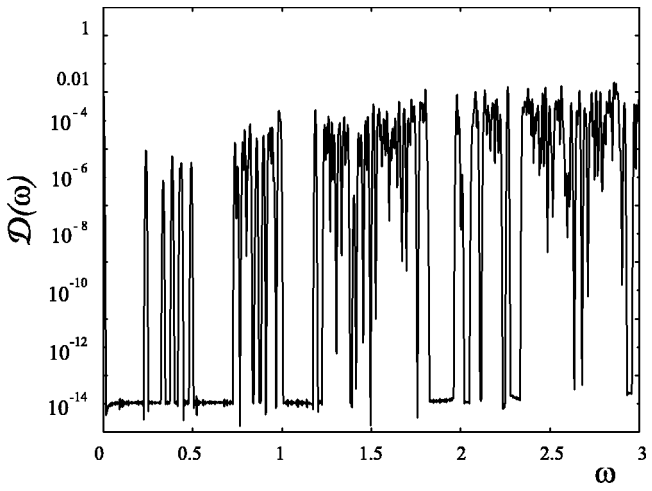

FIG. 12. Density of states of a sample of photonic band-gap material used in Fig. 11. Size of the sample: 9.1×12.1; filling factor: 0.77.

may be confirmed and refined by making more runs. As an example, we consider a system consisting of a dielectric material pierced by air-filled cylinders [37]. The geometry is taken to be a square parallelepiped of size $L=45.1$ that is infinitely extended in the z direction and hence is effectively two dimensional. In Fig. 10, we present the results for the PBGs that we obtained for both the transverse magnetic (TM) and transverse electric (TE) modes as a function of the filling fraction. The data have been generated by means of the algorithm $U_4(\tau)$ with a mesh size $\delta=0.1$ and a time step $\tau=0.1$. To compute the DOS, we used $N=32\,768$ samples of $f(t)$ at time intervals $\Delta t=0.1$. Only a single random initial state for the EM fields has been used. Replacing the free-end boundary conditions Eq. (5) by periodic boundary conditions (results not shown) only leads to minor changes in the locations of PBG's. The results shown in Fig. 10 are in good agreement with those presented in Ref. [37].

In Fig. 11, we study the propagation of time-dependent EM fields through the above-described PBG material consisting of twelve unit cells. The PBG material is placed in a cavity that contains a point source (located to the left of the PBG material) that emits radiation with frequency ω. The TDME were solved by the $U_2(\tau)$ algorithm with $\delta=0.1$ and $\tau=0.01$ in the presence of a current source according to Eq. (58). The snapshots show the absolute intensity E_z^2 of the TM mode at $t=102.4$. The computed DOS of the PBG material is given in Fig. 12. We used the $U_4(\tau)$ algorithm with $\delta=0.1$, $\tau=0.1$, and took $N=32\,768$ samples of $f(t)$ at time intervals $\Delta t=0.1$ in this computation. The presence or absence of gaps in the DOS leads to qualitative changes in the transmitted (and reflected) intensities. Since a gap is present in the DOS at $\omega=1.89$, radiation with this frequency does not easily propagate through the (thin slice of) PBG material. On the other hand, the DOS has no gaps at $\omega=1.50$ and $\omega=2.50$, so that propagation of EM fields through the PBG material should be possible, as is indeed confirmed by Fig. 11.

TABLE I. Frequencies of the eigenmodes of a cubic cavity of size $L=5$. Simulation: values determined from DOS data generated using $U_2(\tau)$ with parameter values $\delta=0.2$, $\tau=0.01$, $N=4096$, and $\Delta t=0.1$.

(k,l,m)	ω_{klm}	Simulation
1,1,0	0.889	0.889
1,1,1	1.088	1.089
2,1,0	1.405	1.404
2,1,1	1.539	1.534
2,2,0	1.777	1.771

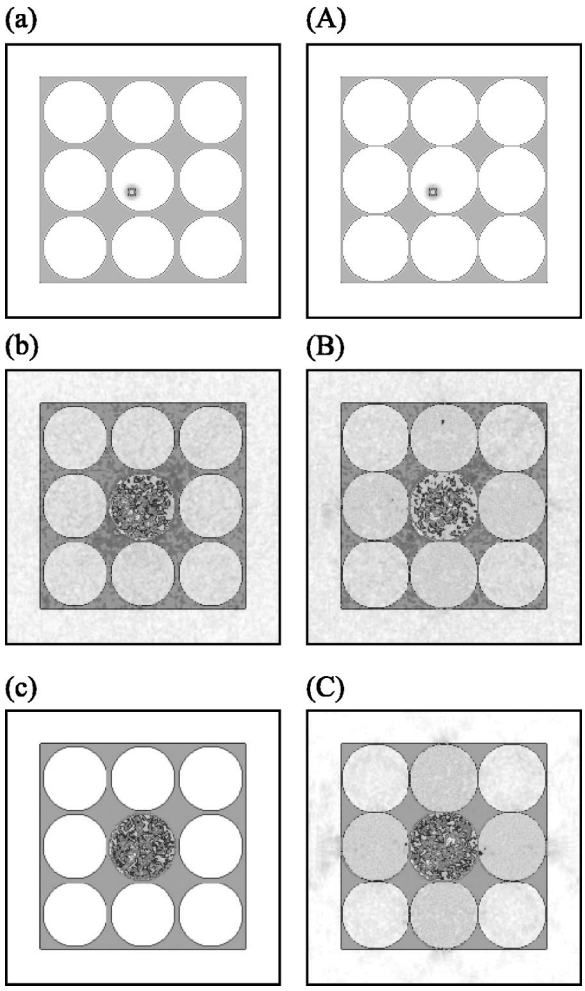

FIG. 13. Intensity of the EM fields in and outside a cubic sample of dielectric material containing $3\times3\times3$ spherical voids, placed in an empty cavity. The size of the cavity is $12.1\times12.1\times12.1$, the size of the sample is $9.1\times9.1\times9.1$, the source is located at (5.6,5.5,6), the slices shown are at $z=6$, the fourth-order algorithm $U_4(\tau)$ was used with a time step $\tau=0.075$ and mesh size $\delta=0.1$. (a): Intensity at $t=0.3$. The radius of the empty spheres is 1.4. (b): Intensity at $t=384$. Same system as in (a). The permittivity of the dielectric material $\varepsilon=1.5$. (c): Intensity at $t=384$. Same system as in (b). The permittivity of the dielectric material $\varepsilon=5$. (A): Intensity at $t=0.3$. The radius of the empty spheres is 1.5. (B): Intensity at $t=384$. Same system as in (A). The permittivity of the dielectric material $\varepsilon=1.5$. (C): Intensity at $t=384$. Same system as in (B). The permittivity of the dielectric material $\varepsilon=5$.

C. Three dimensions

We first compute the modes of a simple cubic cavity of size L. The eigenfrequencies are given by [1]

$$\omega_{klm} = \pi L^{-1} \sqrt{k^2 + l^2 + m^2}, \tag{66}$$

where k, l, and m are non-negative integers. Eigenmodes corresponding to $(k,0,0)$, $(0,l,0)$, and $(0,0,m)$ are incompatible with the boundary conditions Eq. (5). In Table I, we present the frequencies of the five lowest eigenmodes of a cubic cavity for $L=5$.

The agreement with the theoretical values is satisfactory. Note that as the frequency increases, the deviation from the exact result increases. This is due to the (second-order) finite-difference representation of the spatial derivatives on the grid and is a manifestation of the numerical dispersion mentioned earlier.

As a second 3D example, we consider the emission of the EM radiation from a point source located inside dielectric material containing spherical voids. A projection of the material onto the $x-y$ (or $y-z$ or $x-z$) plane is shown in the top panels of Fig. 13. A point source is placed inside the center void to mimic an atom or molecule that emits a photon. The remaining panels in Fig. 13 show snapshots of the light intensity after an elapsed time $t=384$, for different sizes of the voids and different values of the permittivity. If the latter is larger than five, the images no longer depend on the value of the permittivity (results not shown). For $\varepsilon = 1.5$ [panels (b) and (B)] the EM field easily propagates through the sample and leaves the sample from all sides. This is not the case for $\varepsilon=5$: Radiation may leave the sample only at those locations where there is very little or no dielectric material left. In other words, light emerges from the sample in well-defined directions only. Clearly, much more work is necessary to study the propagation of EM radiation in this system as a function of the material parameters, the system size, and the frequency of the emitted photons.

VII. CONCLUSION

We have introduced a family of algorithms to solve the time-dependent Maxwell equations. Salient features of these algorithms are;

(1) rigorously provable unconditional stability for one-, two-, and three-dimensional systems with spatially varying permittivity and permeability,

(2) the use of a real-space (Yee-like) grid,

(3) the order of accuracy in the time step may be systematically increased without affecting the unconditional stability (in this paper, we limited ourselves to second- and fourth-order schemes),

(4) the exact conservation of the energy density of the electromagnetic field,

(5) easy to implement in practice.

We have presented results for the density of states of simple cavities and photonic band-gap materials. We demonstrated that mathematical properties of the algorithms are such that they may be used to compute the density of states with very good accuracy (limited by the accuracy of the spatial discretization used). We gave some illustrative examples of scattering of waves by photonic band-gap systems. These examples also served to show that our algorithms reproduce known results. The first feature opens up possibilities for applications to left-handed materials [38,39]. We intend to report on this subject in the near future.

Although we believe there is little room to improve upon the time-integration scheme itself (except for using higher-order product formulas), for some applications it will be necessary to use a better spatial discretization than the most simple one employed in this paper. There is no fundamental problem to extend our approach in this direction and we will report on this issue and its impact on the numerical dispersion in a future publication.

The rigorous unconditional stability of the algorithms that we proposed in this paper is a direct consequence of adopting a Suzuki-product-formula approach that preserves the fundamental symmetries of the physical system. In view of the generic character of this methodology, the approach pursued in the present paper should be useful for constructing unconditionally stable algorithms that solve the equations for, e.g., sound, seismic and elastic waves as well.

ACKNOWLEDGMENTS

We thank K. Michielsen for a critical reading of the manuscript and W. Bruns for helpful discussions. This work is partially supported by the Dutch ''Stichting Nationale Computer Faciliteiten'' (NCF).

[1] M. Born and E. Wolf, *Principles of Optics* (Pergamon, Oxford, 1964).
[2] K.S. Yee, IEEE Trans. Antennas Propag. **14**, 302 (1966).
[3] A. Taflove and S.C. Hagness, *Computational Electrodynamics-The Finite-Difference Time-Domain Method* (Artech House, Boston, 2000).
[4] See, http://www.fdtd.org
[5] M. Suzuki, J. Math. Phys. **26**, 601 (1985); **32**, 400 (1991).
[6] W. Harshawardhan, Q. Su, and R. Grobe, Phys. Rev. E **62**, 8705 (2000).
[7] This is due to the specific split up adopted in [6] and not an intrinsic property of the spectral-domain approach.
[8] F. Zheng, Z. Chen, and J. Zhang, IEEE Trans. Microwave Theory Tech. **48**, 1550 (2000).
[9] F. Zheng and Z. Chen, IEEE Trans. Microwave Theory Tech. **49**, 1006 (2001).
[10] G. D. Smith, *Numerical Solution of Partial Differential Equations* (Clarendon, Oxford, 1985).
[11] R. Bellman, *Introduction to Matrix Analysis* (SIAM, Philadelphia, 1997).
[12] G. H. Golub and C. F. Van Loan, *Matrix Computations* (John Hopkins University Press, Baltimore, 1983).

[13] H.F. Trotter, Proc. Am. Math. Soc. **10**, 545 (1959).
[14] M. Suzuki, S. Miyashita, and A. Kuroda, Prog. Theor. Phys. **58**, 1377 (1977).
[15] A.J. Chorin, T.J.R. Hughes, M.F. McCracken, and J.E. Marsden, Commun. Pure Appl. Math. **31**, 205 (1978).
[16] H. De Raedt and B. De Raedt, Phys. Rev. A **28**, 3575 (1983).
[17] H. De Raedt, Comput. Phys. Rep. **7**, 1 (1987).
[18] H. Kobayashi, N. Hatano, and M. Suzuki, Physica A **211**, 234 (1994).
[19] H. De Raedt and K. Michielsen, Comput. Phys. **8**, 600 (1994).
[20] A. Rouhi and J. Wright, Comput. Phys. **9**, 554 (1995).
[21] B.A. Shadwick and W.F. Buell, Phys. Rev. Lett. **79**, 5189 (1997).
[22] M. Krech, A. Bunker, and D.P. Landau, Comput. Phys. Commun. **111**, 1 (1998).
[23] P. Tran, Phys. Rev. E **58**, 8049 (1998).
[24] K. Michielsen, H. De Raedt, J. Przeslawski, and N. Garcia, Phys. Rep. **304**, 89 (1998).
[25] H. De Raedt, A.H. Hams, K. Michielsen, and K. De Raedt, Comput. Phys. Commun. **132**, 1 (2000).
[26] A. Hams and H. De Raedt, Phys. Rev. E **62**, 4365 (2000).
[27] J. H. Wilkinson, *The Algebraic Eigenvalue Problem* (Clarendon Press, Oxford, 1965).
[28] R. Alben, M. Blume, H. Krakauer, and L. Schwartz, Phys. Rev. B **12**, 4090 (1975).
[29] M.D. Feit, J.A. Fleck, and A. Steiger, J. Comput. Phys. **47**, 412 (1982).
[30] H. De Raedt and P. de Vries, Z. Phys. B: Condens. Matter **77**, 243 (1989).
[31] T. Kawarabayashi and T. Ohtsuki, Phys. Rev. B **53**, 6975 (1996).
[32] T. Ohtsuki and T. Kawarabayashi, J. Phys. Soc. Jpn. **66**, 314 (1997).
[33] T. Iitaka and T. Ebisuzaki, Mic. Eng. **47**, 321 (1999).
[34] J.M. Bendickson, J.P. Dowling, and M. Scalora, Phys. Rev. E **53**, 4107 (1996).
[35] E. Yablonovitch, Phys. Rev. Lett. **58**, 2059 (1987).
[36] K.M. Ho, C.T. Chan, and C.M. Soukoulis, Phys. Rev. Lett. **65**, 3152 (1990).
[37] C.M. Anderson and K.P. Giapis, Phys. Rev. Lett. **77**, 2949 (1996).
[38] V.G. Veselago, Usp. Fiz. Nauk. **92**, 517 (1964) [Sov. Phys. Usp. **10**, 509 (1968)].
[39] R.A. Shelby, D.R. Smith, and S. Schultz, Science **292**, 77 (2001).